Article

Journal of the Brazilian Chemical Society

https://dx.doi.org/10.21577/0103-5053.20230195

J. Braz. Chem. Soc. **2024**, *35*, 6, e-20230195 , 1-16

Computational Insight and Anticancer Effect of Cinnamic Acid-Derivative Amide Compounds

Aldo Y. Alarcón-López,[a] *Manuel A. Hernández-Serda,*[a] *Pablo Aguirre-Vidal,*[b] *Luis A. Cárdenas-Granados,*[b] *Víctor H. Vázquez-Valadez,*[c,d] *Pablo A. Martínez-Soriano,*[a] *Paola Briseño-Lugo,*[c] *Ana M. Velázquez-Sánchez,*[a] *Elizabeth Rul-Ramírez,*[a] *María Luisa Jiménez-Jiménez,*[e] *Jared Becerril-Ricco,*[e] *Alhel Adán-Ladrón de Guevara,*[e] *José Manuel Tinajero-Rodríguez,*[e] *Elizabeth Ortiz*[e] *and Enrique Ángeles*[*,a]

[a]*Departamento de Ciencias Químicas, FES Cuautitlán, Universidad Nacional Autónoma de México, Av. 1 de Mayo SN Cuautitlán Izcalli, 54750 Estado de México, México*

[b]*Laboratorio de Química Medicinal y Teórica FESC, Universidad Nacional Autónoma de México, Av. 1 de Mayo S/N Cuautitlán Izcalli, 54750 Estado de México, México*

[c]*Departamento de Ciencias Biológicas FES Cuautitlán, Universidad Nacional Autónoma de México, Av. 1 de Mayo SN Cuautitlán Izcalli, 54750 Estado de México, México*

[d]*QSAR Analytics SA de CV, Tempano 10, Colonia Atlanta, Cuautitlán Izcalli, 54740 Estado de México, México*

[e]*Subdirección de Investigación Básica, Instituto Nacional de Cancerología, Av. San Fernando 22 Colonia Sección XVI, 14080 Ciudad de México, México*

In this research, a meticulous screening process was conducted using four servers: Drug Target Explorer, Swiss Target Predictor, SEA Predictor, and Target Hunter. The primary objective was to identify a series of potential biological targets related to the regulation of cell growth and apoptosis in cancer cells using cinnamic acid derivatives. This study focused on five specific targets, matrix metallopeptidase 9 (MMP9), apoptosis inducing factor (AIF), aldo-keto reductase family 1 member C3 (AKR1C3), aldo-keto reductase family 1 member B10 (AKR1B10), mitogen-activated protein kinase 14 (MAPK14), all of which are well known to play a significant role in cancer cell dynamics. To explore both molecular recognition and molecular dynamics, a series of *in silico* investigations (docking and molecular dynamics) were carried out using a collection of 14 cinnamic acid derivatives, including cinnamic acid phenethyl ester (CAPE) as a notable reference molecule due to its widely recognized anticancer effects. Furthermore, preliminary *in vitro* data revealed a potentially promising cytotoxic effect of (*E*)-*N*-[(3,4-dichlorophenyl)methyl]-3-(4-phenoxyphenyl)-2-propenamide (LQM755) on a human gastric adenocarcinoma cell-line (AGS cells), which are characterized by the overexpression of the MMP9 protein. Therefore, the chemical compound LQM755 provides an initial perspective in the field of cancer therapy.

Keywords: cinnamic acid phenethyl ester, cinnamides, cancer, *in silico*, molecular modeling, drug target fishing

Introduction

The most common cause of death in the world is cancer, which is generally characterized by a change in one or more types of cells during a step in the cell cycle. Nearly 10 million deaths in 2020 were attributable to this disease. According to World Health Organization (WHO) data, the most common cancers in 2020 in terms of new cases and their distribution were the following: 2.26 million cases of breast cancer, 2.21 million cases of lung cancer, 1.93 million cases of colorectal cancer, 1.41 million cases of prostate cancer, 1.20 million cases of skin cancer and 1.09 million cases of gastric cancer.[1] In other words, they are first in the world for the breast and fourth for the prostate. Similarly, breast cancer accounts for 11.7% of all diagnosed cases in women, and the most recent data from GLOBOCAN 2020,[2] show that prostate cancer accounts for 7.3% of all diagnosed cases in men. It is significant to note that, particularly in low- and middle-income countries,[3,4] breast cancer has surpassed lung cancer as the most frequently diagnosed malignancy. As a result, one of the

*e-mail: angeles@unam.mx
Editor handled this article: Paula Homem-de-Mello (Associate)

main interests in the field of health research is the search for novel treatments.

Governments, the pharmaceutical industry, and researchers around the world are very focused on finding effective cancer treatments. Since not every patient responds the same way to hormone suppression, one of the most widely used methods in the healthcare industry, there are several approaches and treatment regimens to address these types of cancer.[5,6] It is well known that both localized and advanced cancer treatments can have unfavorable side effects that reduce the ability of patients to lead fulfilling lives.

The type and stage of cancer, as well as the unique traits of each patient, influence the selection of the best course of action. It is crucial to remember that hormone therapy may not always be successful and that, in these circumstances, other alternative solutions might be taken into account. These options include targeted therapy, which focuses on specific abnormalities present in cancer cells to block their growth and induce cell death; immunotherapy, which uses the immune system to fight cancer; and chemotherapy,[7,8] which uses drugs to destroy rapidly growing cells, including cancer cells. As a result, there are various therapeutic options available for the treatment of cancer, and the best course of action depends on the unique circumstances of a person as well as the stage and characteristics of the disease.[9,10]

The idea behind focusing on proliferative pathways in cancer therapy comes from the fact that cancer cells grow and divide without being controlled. This leads to tumor growth and the spread of cancer to other parts of the body. Proliferative signaling pathways are of paramount importance in the regulation of the cell cycle and the facilitation of cell proliferation. The disruption of these pathways has the potential to stop tumor growth and provide effective treatment modalities for cancer.

Apoptosis is an intrinsic biological phenomenon that occurs within viable cells and performs various essential physiological functions. However, within the framework of cancer, modifications in this process play a role in the advancement of tumors and the development of resistance to established therapies. Consequently, there has been growing momentum in the exploration of new pro-apoptotic drugs for the purpose of cancer treatment. Pharmaceutical agents include a variety of compounds consisting of small molecules administered orally and intravenously, as well as monoclonal antibodies. Currently, a diverse array of potentially efficacious anticancer drugs is being developed, spanning the spectrum from preclinical investigations to rigorous clinical trials. The effectiveness of these treatments is being evaluated both when used alone and in conjunction with other medications. The ongoing investigation in this domain has major significance in broadening the scope of therapeutic alternatives for this particular ailment. The potential efficacy of these treatments suggests a positive outlook for the future, highlighting the imperative to continue to advance research efforts and offering additional options in the fight against cancer.

Anticancer agents have the ability to induce apoptosis, a cellular process that leads to the elimination of cancer cells. Induction of apoptosis is achieved through the disruption of multiple signaling pathways involved in the progression of cancer. Several signaling pathways that are significantly impacted in cancer involve matrix metallopeptidase 9 (MMP9),[11] apoptosis inducing factor (AIF),[12] aldo-keto reductase family 1 member C3 (AKR1C3),[13,14] aldo-keto reductase family 1 member B10 (AKR1B10),[15] mitogen-activated protein kinase 14 (MAPK14).[16] The target MMP9 refers to an enzyme known as matrix metalloproteinase MMP9, which is classified as an extracellular matrix proteolytic enzyme within the larger MMP family. AIF is a member of the oxidoreductase protein family. AKR1C3 and AKR1B10 are members of the aldehyde-ketone reductase family, functioning as aldehyde-reducing enzymes. Finally, it should be noted that MAPK14 is a member of the mitogen-activated kinase family and is involved in processes such as proliferation, mitosis, and apoptosis.

Concerning the group of small molecules that this study discusses, it is important to note that cinnamic acid derivatives and cinnamides may be effective against different types of cancer. These molecules are classified as bioactive compounds and have been extensively studied as a result of their potential therapeutic properties. Cinnamide derivatives are chemical compounds derived from cinnamic acid, a naturally occurring substance present in various botanical sources, including cinnamon and propolis. The derivatives under investigation have exhibited notable antitumor efficacy in both preclinical and clinical investigations, thereby establishing their potential as viable contenders for the advancement of novel cancer therapeutic strategies. These molecules have demonstrated various mechanisms of action, such as inhibition of cell proliferation, induction of apoptosis, and suppression of angiogenesis. These mechanisms collectively contribute to their efficacy in the fight against cancer. In a similar vein, the efficacy of cinnamides has been examined in various experimental models, revealing their ability to inhibit cellular proliferation, trigger apoptosis, and inhibit angiogenesis in cancerous cells. Furthermore, cinnamides exhibit synergistic properties when administered in combination with other chemotherapeutic agents, indicating their potential application in combination therapies for the treatment of cancer.[17-21]

In recent years, the field of computational science has made notable progress, greatly influencing the domain of drug discovery and design. This progress has provided valuable resources to tackle the obstacles related to the creation of effective cancer treatments. The aforementioned technologies have demonstrated a rapid and significant increase, particularly within the framework of the coronavirus disease (COVID-19) pandemic outbreak in 2020. Recently, a significant number of research groups across the globe have focused their attention on the use of computational methodologies, resulting in a multitude of advancements, novel developments, and significant discoveries within the domain of drug design. Two of the most notable computational methodologies utilized in the field are molecular docking[22,23] and molecular dynamics simulations.[24,25] These techniques have shown considerable efficacy in the prediction of binding affinity and mode of action for potential anticancer compounds. These methods allow for a closer look at the molecular interactions between compounds and their therapeutic targets. This makes it easier to develop and improve new drug candidates in a logical way.

Previous studies[21,25-28] have provided evidence supporting the efficacy of compound (*E*)-*N*-[(3,4-dichlorophenyl) methyl]-3-(4-phenoxyphenyl)-2-propenamide (LQM755) in in inhibiting breast cancer growth in the MCF-7 cell line. Furthermore, the compound in question has demonstrated positive effects in lung cancer and has shown hepatoprotective properties in cases of cirrhosis, although these findings have not been disseminated through publication at this time.

In contrast, previous studies have documented the efficacy of cinnamic acid phenethyl ester (CAPE), a natural product, in exhibiting significant biological activity against cervical cancer and leukemia.[29] Additionally, CAPE has demonstrated its potential in combating colon cancer[30] and liver cancer.[31,32]

Experimental

Materials

The following reagents and cell lines were used in the present study: cisplatin (No. P4394, Sigma, Saint Louis, Missouri, USA), 3-(4,5-dimethylthiazol-2-yl)-2,5-diphenyltetrazole bromide (MTT) assays (No. M6494, Invitrogen, Waltham, MA, USA), gastric adenocarcinoma cell-line (AGS cells), MCF7 breast cancer cell line, SiHa cervical uterine cells, and non-tumorigenic HaCaT epithelial cell line (ATCC, Manassas, Virginia, USA), 96-well plates (No. 701011, NEST, Palo Alto, California, USA), dimethyl sulfoxide (DMSO, No. D12345, Invitrogen, Waltham, MA, USA), and microplate reader (Multiskan MS MCC/340, Labsystems, Vantaa, Finland).

The *in silico* studies were performed on a workstation featuring an AMD ThreadRipper 3960×, 24-Core, 32GB RAM, and an Nvidia RTX 2070 Super graphic card.

Methodology

Target fishing

Building upon this prior knowledge and the assumption that structural similarity between molecules can indicate similar biological functions, including receptor-ligand interactions, four specialized servers for discovering biological targets were employed: SEA (Similarity Ensemble Approach),[33] Drug Target Explorer,[34] TargetHunter,[35] and Swiss Similarity Search.[36] These servers utilized a total of 52 structures from the LQM700 series molecules and CAPE as input to conduct similarity searches. The 52 structures of the amide-derived compounds were used as queries on the servers to generate a list of potential biological targets, guided by the known activity of the CAPE and LQM755 compounds.

Molecular docking

An internal database containing potential cancer targets was established using the biological targets obtained during the search. Subsequently, a search was conducted in the Protein Data Bank (PDB) database to identify well-defined structures with appropriate parameters for each biological target.

Once the desired PDB structure was obtained, it was prepared using Molecular Operating Environment software 2022.02 (MOE).[37] Missing hydrogen atoms were added, and the absent segments were modeled accordingly. Water molecules not involved in binding interactions were removed to facilitate the calculation of ligand-receptor binding. Subsequently, molecular docking was performed using the Amber:12EHT force field. During this process, 300 conformations of each ligand were considered, applying a rigid receptor profile and the London dG scoring function. Finally, 150 refined conformations were selected, and GBVI/WSA dG was used to calculate the affinity energy of each LQM700 molecule.

Once the docking calculations were completed, the affinity energies of each compound toward the previously identified biological targets were evaluated. Complexes with the highest affinity were chosen; the criteria for selection were mainly the binding energy.

Molecular dynamics simulation

The systems of the complexes with the highest affinity

were set up so that their behavior in molecular dynamics could be compared. The systems were prepared using MOE and solvated in a periodic box with a margin of 10 Å (obtaining boxes of approximately 85 Å size). Additionally, Na^+ ions were added to stabilize any nonneutral charges, and the system was initially minimized in its starting position at a pH of 7. Subsequently, molecular dynamics simulations were performed using Nanoscale Molecular Dynamics 2.13 software (NAMD)[38] and the internal forcefield from MOE Amber12:EHT following a heating and equilibration protocol with a period of 5 ns, followed by a production run of 100 ns in an NVT ensemble. To analyze the molecular dynamics trajectories, the RMSD (root-mean-square deviation), RMSF (root-mean-square fluctuation), and RoG (radius of gyration) of the protein and alpha carbons of the structure for each system were calculated using the initial structure. This step provided valuable information on the behavior of the most energetically favorable LQM700 compound. This comprehensive process aimed to identify promising drug targets for LQM700, with potential implications for the development of novel and effective cancer treatments.

Cell viability assay

Cisplatin was used as a positive control for cell death using MTT assays in human gastric adenocarcinoma cell-line (AGS) cells, MCF7 breast cancer cell line, SiHa cervical uterine cells, and nontumorigenic HaCaT epithelial cell line. This was done to determine how the LQM755 molecule worked. Cells (1×10^4 cells *per* well) were seeded in 96-well plates and incubated for 24 h at 37 °C in a humidified atmosphere with 5% CO_2. Subsequently, the cells were treated with LQM755 at serial concentrations (1, 10, 20, 40, 80, and 100 μM). After 48 h of treatment, 20 μL of MTT were added to each well and incubated for 3 h at 37 °C and 5% CO_2. After incubation, the MTT-containing medium was removed, and 100 μL of DMSO was added. Finally, the absorbance at 570 nm of each well was determined using a microplate reader. All assays were performed in technical triplicates at three different times. The half maximal inhibitory concentration (IC_{50}) was calculated using Origin Pro[39] software.

Results and Discussion

A total of 52 in-house molecules from the LQM700 series were evaluated as queries within the four aforementioned servers. Following the completion of this similarity search, a diverse array of potential biological targets was revealed. Among these, those exhibiting ligands similar to LQM700 were carefully chosen and subsequently enumerated in Table 1. This process of choosing targets involved a thorough analysis of each target taken from lists made by the server, with a focus on how they are related to cancer-related things such as homeostasis, dysregulation, and gene overexpression.

Molecular docking studies were performed individually between each receptor and the 52 molecules of the LQM700 series. The validation of the docking protocol was obtained after a redock of the cocrystallized ligands into the cavity of each receptor. Protein structures were prepared and protonated at pH 7, and missing segments were added when necessary, using the MOE QuickPrep module. Throughout this process, docking scores were meticulously assessed to identify the optimal molecules for binding to the designated targets. The 14 selected structures are presented in Table 2.

Table 3 shows the affinity energy values for each of the biological targets, highlighting, in particular, the data related to LQM755 and CAPE as reference points, for which there is experimental information from preliminary

Table 1. Potential biological targets found during the similarity search to LQM700 series

Target	Expression and activity	PDB ID	Resolution
MMP9	calcium and zinc-dependent metalloprotease overexpressed in various types of cancer; regulates morphogenesis and metastasis processes	6ESM	1.1
AIF	apoptosis-inducing factor; induces caspase-independent programmed cell death	1M6I	1.8
AKR1C3	aldo-keto reductase 1C3; overexpressed in castration-resistant prostate cancer	5HNT	2.0
AKR1B10	aldo-keto reductase 1B10; overexpressed in breast cancer and promotes tumor growth and metastasis	4GQ0	2.1
MAPK14	mitogen-activated protein kinase 14; associated with various cellular processes including proliferation, differentiation, transcription, regulation, and cellular development	5LAR	1.5
EGFR	it is one of the most relevant therapeutic targets in the treatment of lung cancer; it can activate the NF-Kappa-β signaling cascade	6S9B	3.25

PDB: Protein Data Bank; MMP9: matrix metallopeptidase 9; AIF: apoptosis inducing factor; AKR1C3: aldo-keto reductase family 1 member C3; AKR1B10: aldo-keto reductase family 1 member B10; MAPK14: mitogen-activated protein kinase 14; EGFR: epidermal growth factor receptor; NF-Kappa- β: nuclear factor kappa-light-chain-enhancer of activated B cells.

research on their antineoplastic properties. When examining the results, it is evident that LQM755 ranks second to fourth in terms of affinity for the selected targets. Importantly, LQM755 consistently outperformed CAPE in all cases, except for its interaction with the biological AKR1C3 and MAPK14 targets.

As can be observed in Figure 1, from the box and whisker diagram, the criteria to select the theoretically most stable complex based on the binding affinity and its deviation was extended. Based on the observed trend in the values, it was evident that the most favorable compounds are LQM721, LQM753, LQM752, and LQM755 and that the best interaction energy for the most suitable conformations is found with the MMP9 protein. Focusing on this target, 70 molecular recognition conformations within the binding site for each ligand and MMP9 to evaluate the average and deviation of the docking score values were selected, confirming the affinity trend of the three compounds.

MMP9 is one of the most extensively studied metalloprotease endopeptidases. Its role as a key mediator in tumor development has been revealed, exerting an influence on multiple aspects, such as extracellular matrix remodeling, the transition from epithelial cells to mesenchymal cells, cell migration, angiogenesis, and the immune response. Furthermore, elevated levels of this protein have been detected in a variety of tumor types, including esophageal squamous cell carcinomas,[40,41] breast cancer, and breast fibroadenoma.[42] These levels have been associated with an adverse prognosis in cancer-positive individuals, prompting the investigation of MMP9 as a prospective indicator for breast, colorectal, ovarian, and lung cancer. Moreover, it is important to mention that the AKR1B10 and AKR1C3 proteins follow MMP9 in the trend toward increased interaction with ligands, which led to the inclusion of molecular dynamics studies.

The subsequent phase of our computational research was to elucidate the molecular determinants underlying

Table 2. 2D selected structures of LQM700 compounds to study the binding interaction with biological targets

Compound	Structure	Compound	Structure
CAPE	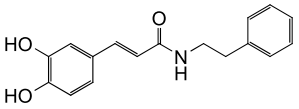	755	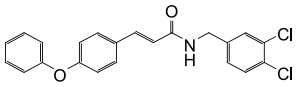
753	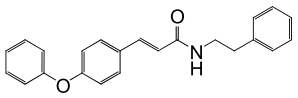	752	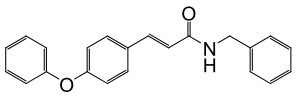
749	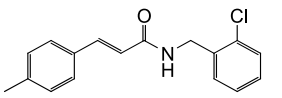	748	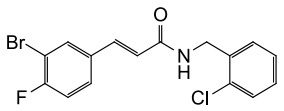
745	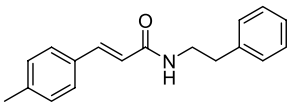	739	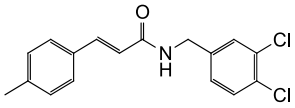
738	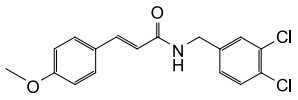	732	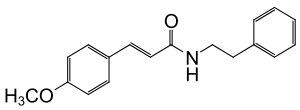
731	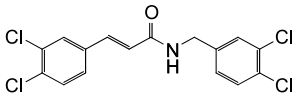	725	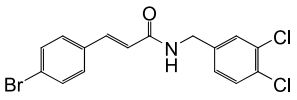
721	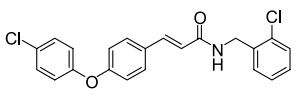	716	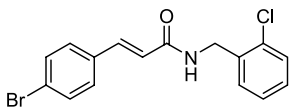
709	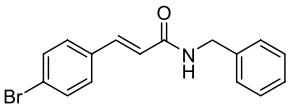	706	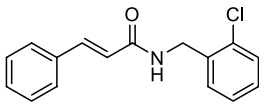

CAPE: cinnamic acid phenethyl ester.

Table 3. Molecular recognition affinity energy results between LQM-700 and the potential biological targets

LQM	MMP9 / (kcal mol^{-1})	LQM	AKR1B10 / (kcal mol^{-1})	LQM	AKR1C3 / (kcal mol^{-1})
753	–9.2937	753	–8.5108	CAPE	–7.8452
752	–9.1993	755	–8.2366	755	–7.6535
755	–9.068	752	–8.1742	721	–7.6482
721	–8.7204	738	–7.8042	753	–7.3802
732	–8.0194	721	–7.6554	738	–6.9837
748	-7.9705	739	–7.5708	725	–6.8119
CAPE	–7.9659	CAPE	–7.5612	732	–6.8047
739	–7.9541	732	–7.5596	739	–6.7611
725	–7.9261	749	–7.3401	748	–6.7021
738	–7.8676	748	–7.2529	731	–6.6903
709	–7.6843	709	–7.1662	709	–6.5556
749	–7.5988	706	–6.9568	716	–6.4586
731	–7.5513	725	–6.9491	749	–6.4426
716	–7.4433	716	–6.75	752	–6.3178
706	–7.3156	731	–6.6597	706	–6.2503
LQM	AIF / (kcal mol^{-1})	LQM	MAPK14 / (kcal mol^{-1})	LQM	EGFR / (kcal mol^{-1})
721	–7.5427	752	–6.7386	721	–7.1207
753	–7.4419	753	–6.7316	753	–7.1038
755	–7.3899	CAPE	–6.6852	755	–7.0451
752	–6.9816	755	–6.5454	752	–6.7265
738	–6.8788	738	–6.5382	738	–6.295
725	–6.7634	721	–6.3703	748	–6.2288
739	–6.7224	748	–6.3608	725	–6.158
748	–6.5757	725	–6.2081	739	–6.1377
732	–6.5276	731	–6.155	732	–5.9571
731	-6.4336	739	–6.1318	CAPE	–5.9017
716	–6.4003	709	–6.1293	731	–5.8873
749	–6.3691	732	–6.0822	749	–5.8701
CAPE	–6.3161	716	–6.0052	706	–5.7535
709	–6.1942	706	–5.8138	709	–5.6816
706	–6.1264	749	–5.525	716	–5.1981

The color scale highlight trends in the binding affinity energies. PDB: protein data bank; MMP9: matrix metallopeptidase 9; AIF: apoptosis inducing factor; AKR1C3: aldo-keto reductase family 1 member C3; AKR1B10: aldo-keto reductase family 1 member B10; MAPK14: mitogen-activated protein kinase 14; EGFR: epidermal growth factor receptor; CAPE: cinnamic acid phenethyl ester.

the antineoplastic efficacy of LQM755, a compound that has been experimentally shown to exhibit activity against cervical cancer, as previously reported. The MMP9, AKR1B10, and AKR1C3 receptors were chosen based on their superior affinity values within the LQM700 series.

Figure 2 shows the outcome of the molecular dynamics of the three receptors (MMP9, AKR1B10 and AKR1C3) bound to the LQM755 ligand. Throughout the simulation, which lasted for 100 ns, the three complexes maintained clear stability, as the average deviation did not exceed 2.5 Å. The MMP9 protein, whose RMSD is depicted in Figure 2 in red, reveals that the ligand undergoes fluctuations at 20 ns due to a conformational change within the protein. These fluctuations reach approximately 2.3 Å. Subsequently, after 30 ns, these fluctuations decrease, and at 40 ns, the average deviation of the complex abruptly increases, reaching 2.1 Å. This deviation remains constant from 40 to 75 ns, a period during which relative stability in the system is observed. After 75 ns, the mentioned deviation decreases to 1.8 Å, remaining nearly constant at ± 0.2 Å for the rest of the simulation.

In the case of the complex with the AKR1B10 protein, which promotes tumor growth and metastasis, a significant fluctuation is observed at 20 ns, with an RMSD value of 2.2 Å. Similarly, after reaching 35 ns, the RMSD decreases for a short period of time, only increasing again to 2.2 Å. When it reaches 60 ns, it decreases once more to 1.6 Å. Beyond this point, there is only a slight increase of 0.3 Å,

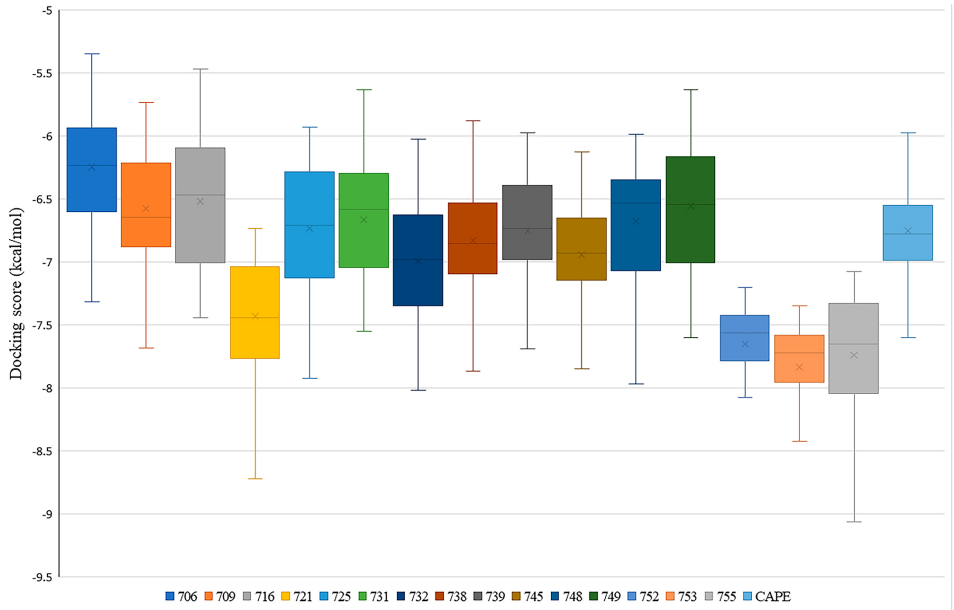

Figure 1. Energy of LQM700 in complex with MMP9. The average and deviation of the interaction energy obtained by molecular docking of LQM700 with the MMP9 complex are presented as a box and whisker diagram. It should be noted that LQM755, 753, 752 and 721 have better values of binding interaction.

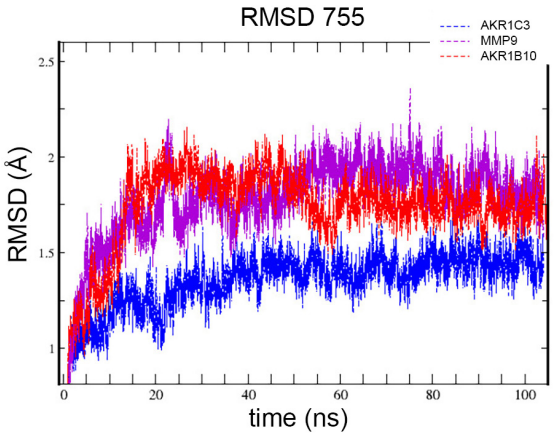

Figure 2. RMSD of protein complexes with LQM755. Blue is AKR1C3; purple is MMP9; and red is AKR1B10 in the molecular dynamics simulation at 100 ns. There are several fluctuations in the quantity that could be present due to conformational changes.

and the RMSD remains stable at approximately 1.7 Å until the end of the simulation. These RMSD changes stem from the ligand's conformational adjustments within the binding site, with the aim of achieving stability with the protein. Finally, in Figure 2, the AKR1C3 protein is depicted in blue, which is associated with castration-resistant prostate cancer. Among the three modeled proteins, it has the lowest RMSD in the entire system, with a value of approximately 1.4 Å for most of the simulations.

The structure of the system was analyzed based on the conformation of the AKR1B10 protein during time intervals in which the RMSD exhibited minor fluctuations. Figure 3a provides a 3D perspective of the amino acids that interact with the LQM755 ligand. In the 2D representation shown in Figure 3b, the interaction of Gln186 and Ser162 with the carbonyl oxygen and amide nitrogen of the ligand through hydrogen donor-acceptor interactions is notable. This interaction remains consistent from a three-dimensional perspective (Figure 3a) throughout the simulation.

Furthermore, it was observed that His113 and Trp1144 have the potential for π-type interactions with the di-chloro-substituted aromatic ring of the ligand. Although not directly observable, the complementarity of the ligand within the binding site is evident. Other residues, such as Ser302 and Tyr212, contribute to effectively encapsulating the ligand within the binding site. Furthermore, the residues that cover the ligand, including Ser213, Lys265, Cys301, and Trp23, are relevant, as they maintain interactions with LQM755 throughout the simulation. The 2D representation with the dashed line shows how the ligand remains well covered by the surrounding amino acids.

Figure 4a shows the RMSF of the AKR1B10 protein with the LQM755 ligand, providing a comparison of the relative flexibility of different regions within a system. Significant fluctuation regions were observed in the interactions, with three that stand out. The first region encompasses residues Leu78 to Trp80, which, due to their presence at the binding site, may exhibit slightly less flexibility compared to neighboring residues. This is attributed to the stability of the ligand interaction, causing them to undergo only minimal and practically significant positional changes without destabilizing the protein structure. The fluctuation in this region reaches approximately 0.5 Å.

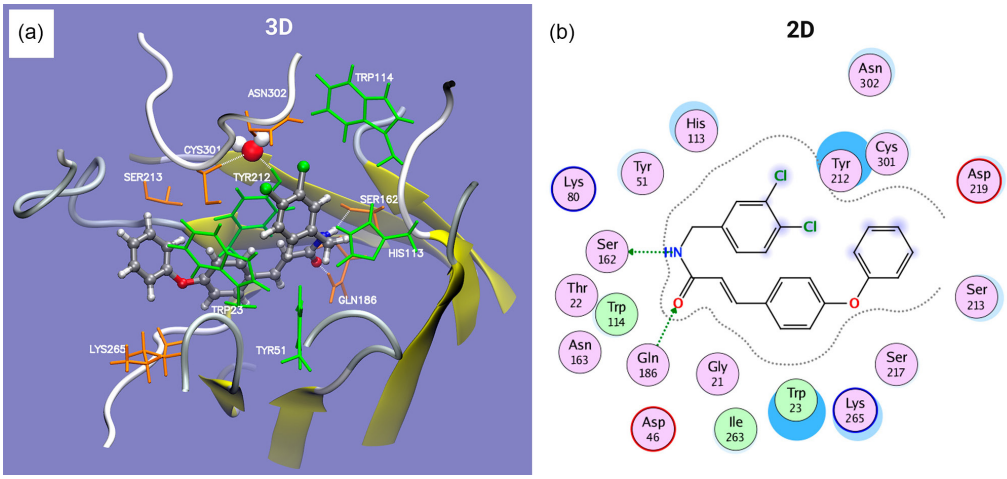

Figure 3. (a) 3D visualization of LQM755 in the AKR1B10 protein, displaying the residues that interact with the ligand, including Trp23, Tyr51, His113, Trp114, Ser162, Gln186, Ser213, Lys265, Cys301, and Asn302. (b) 2D visualization of the LQM755 ligand, highlighting the hydrogen bond donor-acceptor interactions involving the ligand's amide group and the residues Ser162 and Gln186.

The second region includes amino acids His113 and Trp114, which are also found in the binding site and display high affinity for the aromatic rings of the ligand, as mentioned earlier. This contributes to controlled distance fluctuation, maintaining stability. The fluctuation in this region also does not exceed 0.5 Å.

Last, the final region observed involves residues close to Lys265, with its structure resulting in a larger contact area with the ligand. Once again, this translates into minimal fluctuation, mirroring the patterns seen in the two previous regions, thus justifying the stability of the AKR1B10-LQM755 complex.

The stability achieved by LQM755 with the AKR1C3 protein is attributed to the arrangement of the dichlorophenyl ring within the binding site, so that in the complex, this ring stacks with Phe306 to form a π-π stacking interaction. This arrangement can be observed in Figure 5a. It is worth noting that in Figure 5b, the dashed line indicating ligand coverage at the binding site almost completely surrounds the ligand. Due to the lipophilic nature of nearby amino acids such as Leu49, Trp81, Phe 204, Tyr211, Trp222, Phe301, and Phe306, it can be stated that while there are no significant intermolecular interactions such as hydrogen bonds, stability arises from the lipophilic affinity and geometric complementarity between the ligand and the receptor.

Other amino acids that establish π-type interactions include Tyr211, which forms a π-hydrogen interaction with an LQM755 phenyl ring, and Tyr50 and Tyr19, which are located near another phenyl ring. Furthermore, Ser212 was observed to interact with the ligand through hydrogen bonds.

Figure 4b shows the RMSF of the AKR1C protein. It is crucial to consider whether the flexibility of the residues

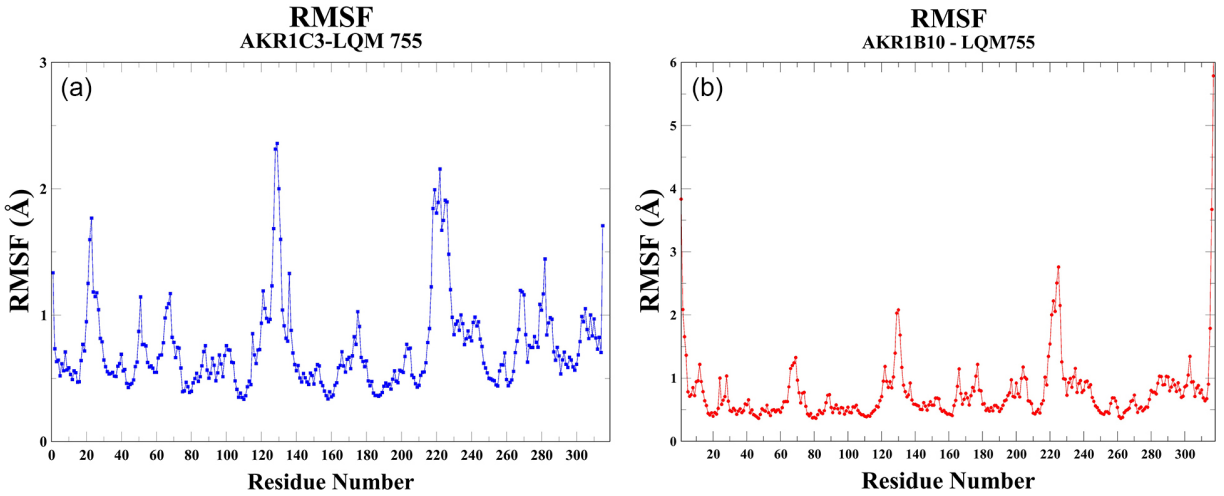

Figure 4. (a) RMSF of the AKR1C3 protein with the LQM755 ligand; the attention can be directed towards regions near to Trp23, TyrR51, His113, Trp114, Ser162, Gln186, Ser213, Lys265, Cys301, and Asn302 to understand the fluctuations of the nearest residues to the ligand. (b) RMSF of the AKR1B10-LQM755 complex in a 100 ns molecular dynamics simulation. We can focus on the regions near Leu49, Trp81, Phe 204, Tyr211, Trp222, Phe301, and Phe306, which interacts with the ligand.

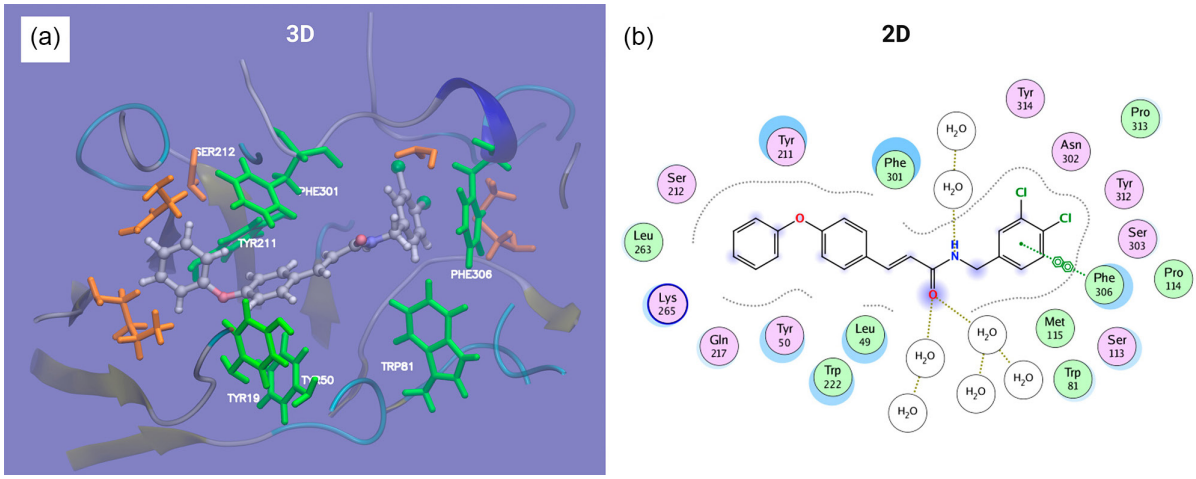

Figure 5. (a) 3D representation of the interaction between LQM755 and the AKR1C3 protein, displaying the residues Phe306, Trp81, Tyr50, Tyr19, Tyr211, and Ser212 involved in the ligand interactions. (b) 2D representation of the LQM755 ligand with the Phe306 residues that engage in a π-type interaction and hydrogen bonding facilitated by the water molecules in the system.

plays a decisive role in the interaction with the ligand. As time progresses, the interactions between the protein and ligand become more pronounced, thereby magnifying their significance for the stability of the ligand. The graph identified five regions, and a detailed analysis of their fluctuations was performed.

The first region is composed of residues close to Tyr19, with a variability of approximately 0.5 Å for this residue. Although it is an aromatic residue, it has the ability to establish a dipole-type interaction with the phenoxy group. It is intriguing to note that the residues adjacent to tyrosine display significant fluctuation, which could have an impact on the interaction with the ligand in this region.

In the second and third regions where the Leu49 and Tyr50 residues are located, the observed variation is also minimal, indicating a slight conformational change. As shown in Figure 5a, both residues are close to the phenoxy group but are oriented more toward the aromatic rings of the ligand, which could lead to π-hydrogen type interactions.

The fourth region is shown as a peak and encompasses a series of amino acids ranging from residues 118 to 131. In the protein structure, these amino acids are arranged in a loop (an irregular sequence of amino acids connected to each other, not adopting secondary structures). During the simulation, this region exhibits higher flexibility and significant movements; however, these do not compromise the structural integrity of the protein.

The next region that deserves consideration encompasses the Tyr211 and Ser212 residues. As mentioned above, tyrosine residues have the potential to establish π interactions with the LQM 755 ligand, explaining the low fluctuation in this area. Additionally, the Ser212 residue features a hydroxyl group capable of forming hydrogen bonds with the ligand. It is also important to highlight the Phe306 residue, as in this binding site region, a noticeable conformational change occurs in the receptor over the course of the simulation. Over time, Phe306 undergoes a spatial adjustment to establish a π-π stacking interaction with the dichlorophenyl group of LQM755. The fluctuation of this loop is approximately 1 Å. This interaction ranks among the most significant in the AKR1C3-LQM755 complex.

Compared to MMP9, it is plausible that there is a lower affinity for the ligand with AKR1C3 and AKR1B10, mainly due to ion-dipole interactions, which depend on the proximity to the ion, its charge, and the dipole moment of the molecule. AKR1C3 and AKR1B10 exhibit weaker interactions than each other. This can also be supported by the docking results.

To go deeper into the examination of the selected complex between MMP9 and LQM755, a structure of MMP9 obtained from the PDB database was used, this included a cocrystallized inhibitor ((2*S*)-2-[2-[4-(4-methoxyphenyl) phenyl]sulfanylphenyl]pentanedioic acid), also known as B9Z,[40] and modeled the interaction at the corresponding binding site. The crystal structure with the ligand inside was minimized with a molecular mechanics method using AMBER12:EHT in MOE to achieve a relaxed structure of the complex. The two-dimensional interactions are depicted in Figure 6. The key amino acids involved in the interactions are Tyr423, Arg424, and Leu187 with polar π-H interactions and Leu188 with a polar interaction. The zinc atom also keeps the ligand in the pocket due to an ion-dipole interaction.

It is important to note that the number of amino acids in PDB 6ESM differs significantly from the entire MMP9 sequence. This discrepancy arises because the amino acids that make up the catalytic site are not arranged in a

single consecutive sequence. In fact, there is an absence of 175 amino acids in the model, from 217 to 391. To maintain consistency with the amino acids involved in the primary interactions with ligands, the sequence numbering corresponding to the full sequence found in UniProt entry P14780 was adopted. Additionally, the model contains a Glu to Gln mutation at position 402.

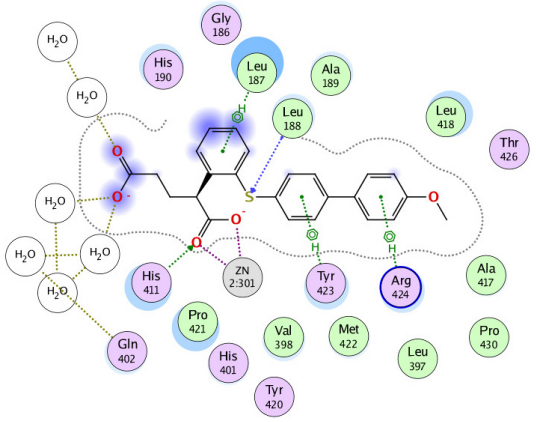

Figure 6. The ligand BZ9 binds to MMP9 in the crystal structure due to a significant interaction between the zinc atom and His411 and one of the carboxylate groups. This is due to polar π-H interactions between the phenyl groups and Tyr423 and Arg424. The amino acids Leu187 and Leu188 also interact with the ligand.

In comparison, as seen in Figure 7, significant polar (H-π)-interactions were established between LQM755 and a hydrogen atom in Leu418, it should be mentioned that even when Tyr423 did not have an interaction with an aromatic group, it remained close to the ligand. It is important to note that Leu187 and Leu188 also interact with LQM755 in a double π-H interaction, similar to how BZ9 interacts with the protein. Furthermore, a zinc-mediated interaction was observed, as expected, since the activity of the metalloprotease is based on this element.

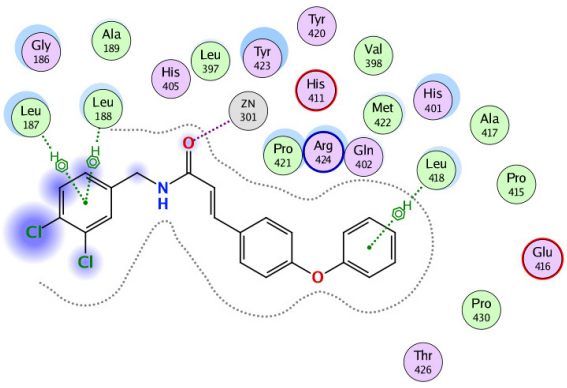

Figure 7. This figure highlights crucial interactions involving compound LQM755 and MMP9. Tyr423 is still close to the ligand and Zn has an important interaction with the carbonyl oxygen from the amide compound. Important interactions are formed between Leu418, Leu187, and Leu188 and the ligand.

This interaction enhances the stability of the complex because of the strong ion-dipole interaction with the oxygen of the amide group in the ligand. Along the dashed line, it is evident that the ligand is partially enveloped by the receptor's molecular surface, except in the region of dichlorophenyl. The violet-colored area indicates the exposure of the ligand to the receptor's molecular surface, suggesting that the dichlorosubstituted ring is positioned outside the binding pocket. However, the phenoxy group remains predominantly concealed by the molecular surface, which implies its deeper integration within the receptor.

In molecular dynamics simulations, three parameters were evaluated using Visual Molecular Dynamics 1.9.3 software (VMD).[43,44] The first was RMSD for the LQM755 complex in MMP9 in an extended simulation of 500 ns, as shown in Figure 8a. The simulation was found to be stable during production time, and its value is consistent with conventional ranges of motion, suggesting that an RMSD of 2.5 Å is a good indicator of equilibria. The radius of gyration was also analyzed to confirm stability (Figure 8c), indicating that the compactness of the protein is stable throughout the simulation and that the protein does not have an important deformity, indicating probable denaturalization of the protein.

RMSF indicated an interesting motion of the residues involved in binding with LQM755. It can be seen that the residue numbers involved in the binding site, corresponding to Leu187 and Leu188, show a low deviation from their initial positions and that the region comprising Met422, Tyr423, and Arg424 has a higher fluctuation. The region with a greater deviation can be seen in the RMSF plot in the region around residue Tyr423. In Figure 8a, the achievement of equilibrium is clearly observed with a measurement of 2. Moving our focus to Figure 8b, our attention is directed toward residues 187-190, 214-216, and 422-425 (green regions and red line), which play a critical role at the binding site. In particular, these regions exhibit significant fluctuations, revealing marked flexibility.

In Figure 8c, it is evident that the compact structure of the protein maintains its stability, showing no signs of denaturation. In Figure 8a, two distinct regions in the RMSD are noticeable: the higher values (2 Å) correspond to an open conformation of the complex, while the lower value is associated with a closed conformation (1.75 Å). The difference between the two conformations lies in the change in loop regions in the protein, specifically one of the terminal loops in the structure, which is highly flexible.

In Figure 9, it is possible to appreciate the superposition of two average structures from the simulation. Focusing on the regions of RMSD values mentioned above, the green protein corresponds to the open conformation of the

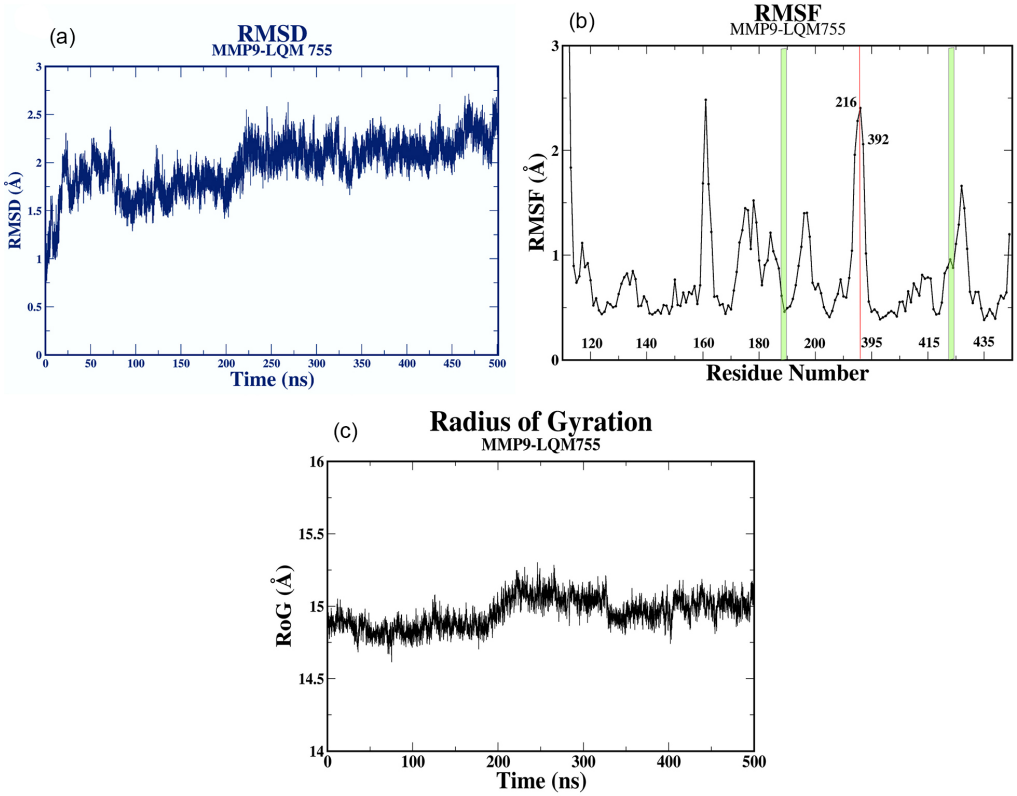

Figure 8. (a) RMSD of the protein MMP9 during a 500 ns molecular dynamics simulation. Due to a total fluctuation of the protein of less than 2.5 Å between the highest and lowest value, it is possible to consider the dynamics to be stable. (b) RMSF of the protein. The red line indicates the cutoff for the missing residues in the full MMP9 gene, near this region there are residues 214-216 that interact with the ligand. The green regions involve 187-190 and 422-425 that also interact with the ligand. (c) Radius of gyration of the protein; a low change in the value of the compactness of the protein gives a clue on the stability of the tertiary structure.

complex, while the pink/magenta structure belongs to the closed conformation. The figure highlights a significant transformation in the protein topology using lime color, so it become evident that the change in the structure is mainly due to the flexibility of several loop areas that include the regions with a high RMSF in Figure 8b. Additionally, an alteration in the conformation of the ligand can be observed.

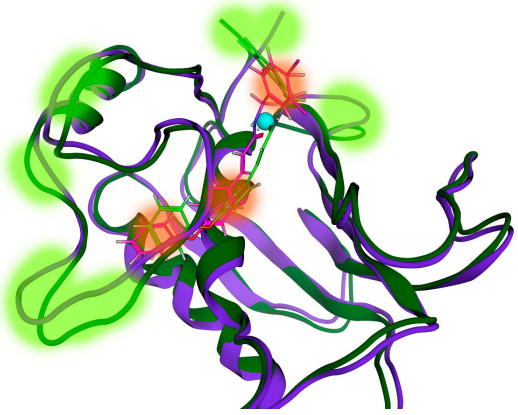

Figure 9. The main changes observed in the RMSD plots in the molecular dynamics of the complex of LQM755 in MMP9 are the result of the sum of changes in several loops (lime regions) and a deviation of the ligand (orange regions).

Even though Zn (in cyan) stabilizes the amide interaction, it becomes clear that the di-chloro-substituted phenyl group has a steric effect on the protein, which could be the cause of the change in conformation in that molecular region.

To go deeper into the observations, it is possible to analyze the key amino acids found at the LQM755 binding site in the closed conformation when more intermolecular interactions were observed, as shown in Figure 10. Throughout the simulation, it was observed that the zinc atom remained in its position due to a zinc finger motif, which relies on its interaction with three histidines (depicted in blue). Furthermore, this same metal, in its octahedral geometry (sp3d2), contributes to maintaining the position of the ligand by interacting with the carbonyl oxygen while simultaneously stabilizing the protein's folding. Concurrently, this atom interacted with two water molecules that remained in the same position throughout the simulation, and these molecules also influenced the preservation of the tertiary structure of the protein.

The preservation of the location of the phenoxy group is attributed to its interaction with Met422, Tyr423, Arg424 and Leu418. In this context, leucine molecules that are part of the β-sheet gain importance in relation to the

dichlorosubstituted phenyl group, where the steric effect is more pronounced.

Biological effect

In the field of *in silico* research, the LQM700 series has revealed promising anticancer potential due to its interaction with various biological targets associated with the tumorigenic and metastatic capacity of cancer cells. To evaluate whether compounds from the LQM700 series could be considered candidates for the treatment of different types of cancer, two molecules were selected for preliminary studies using MTT assays.

The first selected molecule was LQM755, which has previously[21] been reported to exhibit anticancer activity by our research group. Furthermore, *in silico* analysis showed that LQM755 ranks second and fourth in affinity with the selected targets, making it a promising candidate for further investigations.

In preliminary studies on the activity of compound LQM755 in AGS cells and noncancerous HaCaT cells (Figure 11), antineoplastic activity was observed along with low cytotoxicity in noncancerous cells.

In vitro, the MTT assay data demonstrated that LQM755 reduced the viability of AGS cells (Figure 11a), showing a projected IC_{50} value of 24 μM (Figure 12a) compared to the IC_{50} of cisplatin of 25 μM, which was used as a comparative and positive drug control for cell death (Figure 12b).

Furthermore, the LQM755 compound did not affect nontumorigenic HaCaT cells (Figure 11b), in contrast to cisplatin, which showed a distinct impact on these types of cells. This suggests that LQM755 could inhibit gastric cancer cells with limited side effects, which must be

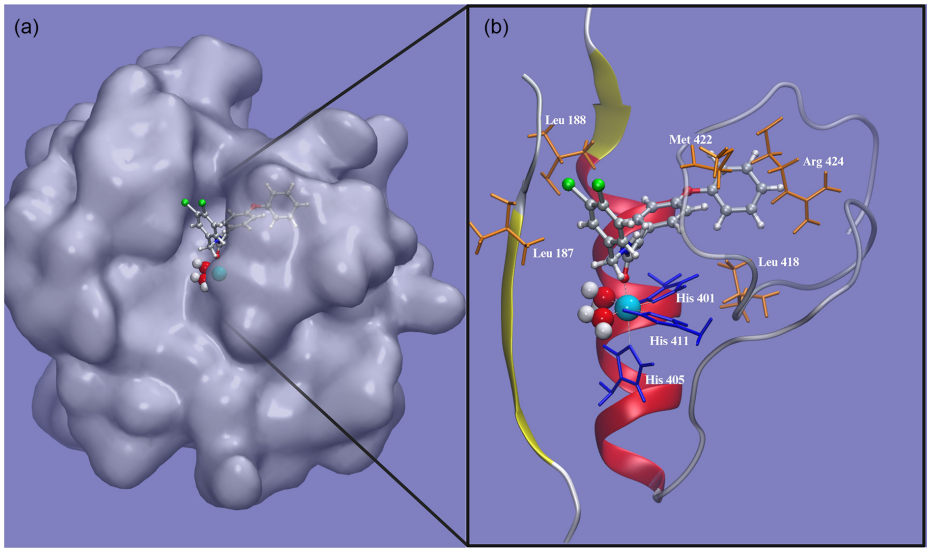

Figure 10. The binding sites of the LQM755 ligand with the MMP9 target in the closed conformation, (a) representation of the complete MMP9 target with the ligand, (b) the pocket of the MMP9 target with the LQM755, ligand where are shown (in blue) HIS401, HIS405, HIS411 in interaction with zinc (in cyan) and LEU187, LEU188, LEU418, MET422, and ARG424 (in orange) in interaction with the LQM755 ligand.

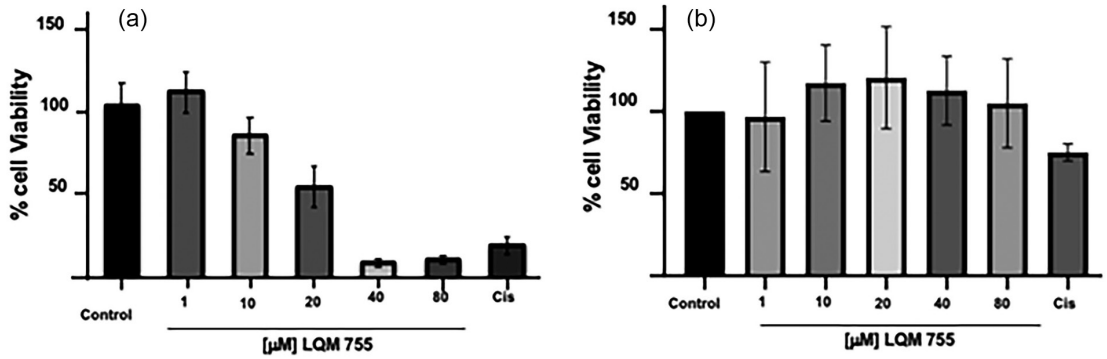

Figure 11. LQM755 decreases the viability of gastric cancer cells. (a) AGS cells were treated with a series of concentrations of LQM755 for 48 h under tissue culture conditions in a dose-response assay; inhibitory concentration of cisplatin resulting in 75% inhibition of cell growth (IC75) was used as a positive control to make cell death evident. (b) Nontumorigenic HaCaT cells were not targeted by the LQM755 molecule. The data were generated by three independent MTT assays.

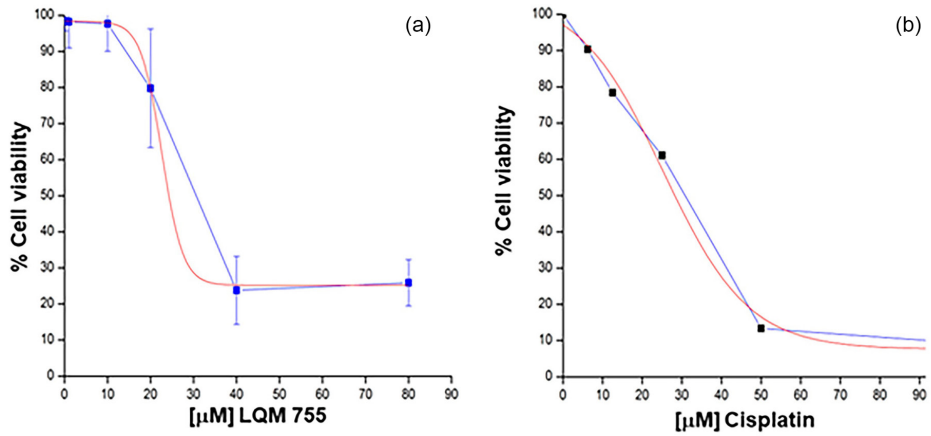

Figure 12. (a) Estimate models for the half maximal inhibitory concentration (IC_{50}) calculation of LQM755 and (b) cisplatin in AGS cells. Dose response data were analyzed by Origin Pro software.[39]

evaluated through robust *in vitro* assays and preclinical studies.

These preliminary studies suggest that LQM755 has promising properties for the development of cancer therapies. However, further in-depth research is required to fully understand their effectiveness and selectivity for different types of cancer cells. These results open new perspectives and opportunities in the search for more effective and safer cancer treatments. Furthermore, considering *in silico* studies, the molecules LQM721, LQM752 and LQM753 could potentially be even more active than LQM755, adding further potential to this line of research. The toxicity studies of this compound and its analogs are currently under evaluation by the group.

Furthermore, *in vitro* data revealed a potentially promising cytotoxic effect of LQM755 on AGS cells. It is important to note that one of the distinctive features of this type of cancer is the overexpression of the protein MMP9,[41,42,45-49] suggesting that the compound may target a relevant molecular pathway involved in the high proliferation of these malignant cells. Additionally, it is encouraging to observe that LQM755 does not affect nontumorigenic HaCaT cells, indicating a possible selectivity of the compound toward cancer cells without causing harm to normal cells.

On the other hand, according to Figure 12, the projected IC_{50} of LQM755 is 24 μM compared to the IC_{50} of cisplatin, which is 45 μM, making it more effective against this type of cancer cell and suggesting its possible use as an antineoplastic treatment once its efficacy is demonstrated in preclinical and clinical studies. In contrast to the considerable side effects of cisplatin,[50,51] LQM755, derived from CAPE), could represent a safer alternative, similar to the natural product CAPE itself.[52-54]

The mechanism by which LQM755 exerts its selective cytotoxic effects is still unknown, and an important part of this study is the direction of research toward this objective. The *in silico* data generated in this work suggest that the effect of LQM755 could be due to its interaction with overexpressed EGFR and MAPK14 proteins, which are relevant in cellular pathways involved in the high proliferation rate of cancer cells. Additionally, docking data showed that LQM molecules interact with MMP9, a relevant enzyme related to metastasis and progression.[55,56] These findings open interesting lines of investigation to better understand the mechanisms of action of these molecules and their selectivity toward cancer cells.

Finally, the data collected to date establish a solid foundation that supports the need for further in-depth investigation into the mechanisms of action and cytotoxic properties of compound LQM755. Its promising anticancer activity and apparent affinity for certain types of cancer cells open up a realm of possibilities in the field of oncology. Furthermore, it should be noted that this study revealed that the LQM721, LQM752 and 753 molecules could potentially outperform CAPE and LQM755 in terms of efficacy, adding an intriguing dimension.

However, to robustly support and validate these findings, it is imperative to carry out a series of additional studies both *in vitro* and *in vivo*. This deeper investigation will bring us closer to the potential therapeutic use of the LQM series as antineoplastic agents in the clinical setting.

The results obtained thus far impart an intriguing character to the series of LQM700 molecules, prompting future approaches aimed at meticulously evaluating their cytotoxic effect on cancer cells. In particular, the possibility of utilizing them in combination with current chemotherapeutic agents and approaches for cancer treatment is emerging. This combined approach holds promise, as it has the potential to minimize damage to noncancerous cells, thus avoiding undesired consequences.

Conclusions

In summary, this study aimed to identify biological targets for a series of amides derived from the phenethyl ester of caffeic acid using similarity-based search servers. A wide range of potential targets related to various conditions and normal biological processes was compiled. Manual analysis of the data obtained led to the selection of targets closely related to apoptosis induction and potential cell cycle effects, specifically AKR1C3, AKR1B10, MMP9, AIF, and MAPK14, particularly in prostate, breast, and lung cancers. X-ray crystallography structures from the PDB database were chosen for these targets and prepared using the Amber12:EHT force field.

Molecular recognition studies highlighted the best docking energies for the LQM700 and MMP9 complex, a protein associated with various types of cancer, including esophageal squamous cell carcinoma, breast cancer, and fibroadenoma. Dynamic molecular simulations of these complexes shed light on their behavior at binding sites. Although the LQM755-AKR1C3 complex appeared more stable with a lower RMSD than the AKR1B10 and MMP9 complexes, this stability resulted from a combination of weaker interactions, such as geometric complementarity and lipophilicity, rather than significant intermolecular interactions, such as the ion-dipole interaction observed in MMP9-LQM755. The AKR1B10 simulation revealed that hydrogen bonding was the most significant interaction, followed by geometric complementarity.

For the MMP9-LQM755 complex, extended molecular dynamics simulations indicated the pivotal role of zinc in stabilizing the LQM700 compounds within the protein. The zinc finger in this metalloprotease and the interaction of the metal with carbonyl oxygen were key supramolecular features that promoted stability.

Acknowledgments

We thank the PAPIIT IN202020 Project, the LANCAD-UNAM-DGTIC-034 Supercomputing Project, the FESC PIAPI CI2201 Project, PAPIIT 206023, and the XVIII Mexico-Quebec Working Group Project, 2021-2023 of Secretaria de Relaciones Exteriores de México and Grant AS1-40601 of CONAHCYT for their support.

Author Contributions

Aldo Y. Alarcón-López was responsible for investigation; Pablo Aguirre-Vidal for validation; Víctor Hugo Vázquez-Valadez for software; Pablo Martínez-Soriano for validation; Manuel A. Hernández-Serda for software; Paola Briseño-Lugo for conceptualization; Luis Alfonso Cárdenas-Granados for software; Ana María Velázquez-Sánchez for data curation; Elizabeth Rul-Ramírez for conceptualization; María Luisa Jiménez-Jiménez for data curation; Jared Becerril-Ricco for data curation; Alhel Adán-Ladrón de Guevara for data curation; José Manuel Tinajero-Rodríguez for data curation; Elizabeth Ortiz for investigation.

References

1. Ferlay, J.; Colombet, M.; Soerjomataram, I.; Parkin, D. M.; Piñeros, M.; Znaor, A.; Bray, F.; *Int. J. Cancer* **2021**, *149*, 778. [Crossref]
2. GLOBOCAN 2020: New Global Cancer Data, https://www.uicc.org/news/globocan-2020-new-global-cancer-data, accessed in November 2023.
3. World Health Organization (WHO); *Cancer*, https://www.who.int/news-room/fact-sheets/detail/cancer, accessed in November 2023.
4. World Health Organization (WHO); *Breast Cancer*, https://www.who.int/news-room/fact-sheets/detail/breast-cancer, accessed in November 2023.
5. American Cancer Society; *Hormone Therapy for Prostate Cancer*, https://www.cancer.org/cancer/types/prostate-cancer/treating/hormone-therapy.html, accessed in November 2023.
6. Focht, B. C.; Lucas, A. R.; Grainger, E.; Simpson, C.; Fairman, C. M.; Thomas-Ahner, J. M.; Buell, J.; Monk, J. P.; Mortazavi, A.; Clinton, S. K.; *Ann. Behav. Med.* **2018**, *52*, 412. [Crossref]
7. Meric-Bernstam, F.; Sweis, R. F.; Kasper, S.; Hamid, O.; Bhatia, S.; Dummer, R.; Stradella, A.; Long, G. V.; Spreafico, A.; Shimizu, T.; *Clin. Cancer Res.* **2023**, *29*, 110. [Crossref]
8. Das, A.; Prajapati, A.; Karna, A.; Sharma, H. K.; Uppal, S.; Lather, V.; Pandita, D.; Agarwal, P.; *Chem.-Biol. Interact.* **2023**, *376*, 110443. [Crossref]
9. Guo, C.; Luo, Z.; Ismtula, D.; Bi, X.; Kong, H.; Wang, Y.; Yang, Z.; Mao, X.; *Comb. Chem. High Throughput Screening* **2023**, *26*, 639. [Crossref]
10. Liu, S.; Ye, Z.; Xue, V. W.; Sun, Q.; Li, H.; Lu, D.; *BMC Cancer* **2023**, *23*, 307. [Crossref]
11. Li, Y.; Cai, B.; Chen, S.; Fu, X.; Pang, X.; Zhu, X.; Qi, H.; Tan, W.; *J. Cancer. Res. Ther.* **2018**, *14*, S713. [Crossref]
12. Rao, S.; Mondragón, L.; Pranjic, B.; Hanada, T.; Stoll, G.; Köcher, T.; Zhang, P.; Jais, A.; Lercher, A.; Bergthaler, A.; Schramek, D.; Haigh, K.; Sica, V.; Leduc, M.; Modjtahedi, N.; Pai, T. P.; Onji, M.; Uribesalgo, I.; Hanada, R.; Kozieradzki, I.; Koglgruber, R.; Cronin, S. J.; She, Z.; Quehenberger, F.; Popper, H.; Kenner, L.; Haigh, J. J.; Keep, O.; Rak, M.; Cai, K.; Kroemer, G.; Penninger, J. M.; *Cell Res.* **2019**, *29*, 579. [Crossref]
13. Liu, Y.; Chen, Y.; Jiang, J.; Chu, X.; Guo, Q.; Zhao, L.; Feng, F.; Liu, W.; Zhang, X.; He, S.; Yang, P.; Fang, P.; Sun, H.; *Eur. J. Med. Chem.* **2023**, *247*, 115013. [Crossref]
14. Dwivedi, P. S. R.; Shastry, C. S.; *Arabian J. Chem.* **2023**, *16*, 04778. [Crossref]

15. Li, L.; Chao, Z.; Waikeong, U.; Xiao, J.; Ge, Y.; Wang, Y.; Xiong, Z.; Ma, S.; Wang, Z.; Hu, Z.; Zeng, X.; *J. Transl. Med.* **2023**, *21*, 146. [Crossref]
16. Prasher, P.; Sharma, M.; Chan, Y.; Singh, S. K.; Anand, K.; Dureja, H.; Jha, N. K.; Gupta, G.; Zacconi, F.; Chellappan, D. K.; Dua, K.; *Curr. Med. Chem.* **2023**, *30*, 1529. [Crossref]
17. Amano, R.; Yamashita, A.; Kasai, H.; Hori, T.; Miyasato, S.; Saito, S.; Yokoe, H.; Takahashi, K.; Tanaka, T.; Otoguro, T.; *Antiviral Res.* **2017**, *145*, 123. [Crossref]
18. Dutta, A.; Dhara, D.; Parida, P. K.; Si, A.; Yesuvadian, R.; Jana, K.; Misra, A. K.; *RSC Adv.* **2017**, *7*, 28853. [Crossref]
19. Reddy, N. D.; Shoja, M. H.; Biswas, S.; Nayak, P. G.; Kumar, N.; Rao, C. M.; *Chem.-Biol. Interact.* **2016**, *253*, 112. [Crossref]
20. Mielecki, M.; Lesyng, B.; *Curr. Med. Chem.* **2016**, *23*, 954. [Crossref]
21. Martínez-Rosas, J. R.; Díaz-Torres, R.; Ramírez-Noguera, P.; López-Barrera, L. D.; Escobar-Chavez, J. J.; Angeles, E. R.; *Pharmazie* **2020**, *75*, 324. [Crossref] [Link] accessed in November 2023
22. Dnyandev, K. M.; Babasaheb, G. V.; Chandrashekhar, K. V.; Chandrakant, M. A.; Vasant, O. K.; *Int. Res. J. Pure Appl. Chem.* **2021**, *22*, 60. [Crossref]
23. Saikia, S.; Bordoloi, M.; *Curr. Drug Targets* **2019**, *20*, 501. [Crossref]
24. Pamučar, D.; Marinković, D.; Kar, S.; *Mathematics* **2021**, *9*, 1416. [Crossref]
25. Kumari, I.; Sandhu, P.; Ahmed, M.; Akhter, Y.; *Curr. Protein Pept. Sci.* **2017**, *18*, 1163. [Crossref]
26. Sinha, A. K.; Sharma, A.; Joshi, B. P.; *Tetrahedron* **2007**, *63*, 960. [Crossref]
27. Chen, C.-C.; Ho, J.-C.; Chang, N.-C.; *Tetrahedron* **2008**, *64*, 10350. [Crossref]
28. Martínez-Soriano, P. A.; Macías-Pérez, J. R.; Velázquez, A. M.; Camacho-Enriquez, B. C.; Pretelín-Castillo, G.; Ruiz-Sánchez, M. B.; Abrego-Reyes, V. H.; Villa-Treviño, S.; Angeles, E.; *Green Sustainable Chem.* **2015**, *5*, 81. [Crossref]
29. Chen, J.-H.; Shao, Y.; Huang, M.-T.; Chin, C.-K.; Ho, C.-T.; *Cancer Lett.* **1996**, *108*, 211. [Crossref]
30. He, Y. J.; Liu, B. H.; Xiang, D. B.; Qiao, Z. Y.; Fu, T.; He, Y. H.; *World J. Gastroenterol.* **2006**, *12*, 4981. [Crossref]
31. Carrasco-Legleu, C. E.; Sanchez-Perez, Y.; Marquez-Rosado, L.; Fattel-Fazenda, S.; Arce-Popoca, E.; Hernandez-Garcia, S.; Villa-Treviño, S.; *World J. Gastroenterol.* **2006**, *12*, 6779. [Crossref]
32. Carrasco-Legleu, C. E.; Marquez-Rosado, L.; Fattel-Fazenda, S.; Arce-Popoca, E.; Perez-Carreon, J. I.; Villa-Trevino, S.; *Int. J. Cancer* **2004**, *108*, 488. [Crossref]
33. Keiser, M. J.; Roth, B. L.; Armbruster, B. N.; Ernsberger, P.; Irwin, J. J.; Shoichet, B. K.; *Nat. Biotechnol.* **2007**, *25*, 197. [Crossref]
34. Allaway, R. J.; La Rosa, S.; Guinney, J.; Gosline, S. J. C.; *J. Cheminf.* **2018**, *10*, 41. [Crossref]
35. Wang, L.; Ma, C.; Wipf, P.; Liu, H.; Su, W.; Xie, X.-Q.; *AAPS J.* **2013**, *15*, 395. [Crossref]
36. Bragina, M. E.; Daina, A.; Perez, M. A. S.; Michielin, O.; Zoete, V.; *Int. J. Mol. Sci.* **2022**, *23*, 811. [Crossref]
37. *MOE: Molecular Operating Environment*, v. 2022.02; Chemical Computing Group (CCG), Canada, 2022.
38. Phillips, J. C.; Hardy, D. J.; Maia, J. D. C.; Stone, J. E.; Ribeiro, J.V.; Bernardi, R. C.; Buch, R.; Fiorin, G.; Henin, J.; Jiang, W.; McGreevy, R.; Melo, M. C. R.; Radak, B. K.; Skeel, R. D.; Singharoy, A.; Wang, Y.; Roux, B.; Aksimentiev, A.; Luthey-Schulten, Z.; Kale, L. V.; Schulten, K.; Chipot, C.; Tajkhorshid, E.; *NAMD Molecular Dynamics Software*, v. 2.13; Theoretical Biophysics Group University of Illinois and Beckman Institute, USA, 2018.
39. *Origin(Pro)*, v. 2021 9.8; OriginLab Corporation, Northampton, MA, USA, 2021.
40. Augoff, K.; Hryniewicz-Jankowska, A.; Tabola, R.; Stach, K.; *Cancers* **2022**, *14*, 1847. [Crossref]
41. Augoff, K.; Hryniewicz-Jankowska, A.; Tabola, R.; Czapla, L.; Szelachowski, P.; Wierzbicki, J.; Grabowski, K.; Sikorski, A. F.; *Oncol. Rep.* **2014**, *31*, 2820. [Crossref]
42. Martins, L. M.; Dourado, C. S. D. M. E.; Campos-Verdes, L. M.; Sampaio, F. A.; Revoredo, C. M. S.; Costa-Silva, D. R.; Barros-Oliveira, M. D. C.; Nery Jr., E. D. J. N.; Rego-Medeiros, L. M. D.; Gebrim, L. H.; Alves-Ribeiro, F. A.; Rodrigues, G. P.; Chagas, D. C.; Marreiro, D. N.; da Silva, B. B.; *Oncotarget* **2019**, *10*, 6879. [Crossref]
43. Humphrey, W.; Dalke, A.; Schulten, K.; *J. Mol. Graphics* **1996**, *14*, 33. [Crossref]
44. Humphrey, W.; Dalke, A.; Schulten, K.; *VMD: Visual Molecular Dynamics*, v. 1.9.3; Theoretical Biophysics Group University of Illinois and Beckman Institute, USA, 2018.
45. Nuti, E.; Cuffaro, D.; Bernardini, E.; Camodeca, C.; Panelli, L.; Chaves, S.; Ciccone, L.; Tepshi, L.; Vera, L.; Orlandini, E.; Nencetti, S.; Stura, E. A.; Santos, M. A.; Dive, V.; Rossello, A.; *J. Med. Chem.* **2018**, *61*, 4421. [Crossref]
46. Yoo, Y. A.; Kang, M. H.; Lee, H. J.; Kim, B.-h.; Park, J. K.; Kim, H. K.; Kim, J. S.; Oh, S. C.; *Cancer Res.* **2011**, *71*, 7061. [Crossref]
47. Kubben, F. J. G. M.; Sier, C. F. M.; Hawinkels, L. J. A. C.; Tschesche, H.; van Duijn, W.; Zuidwijk, K.; van der Reijden, J. J.; Hanemaaijer, R.; Griffioen, G.; Lamers, C. B. H. W.; Verspaget, H. W.; *Eur. J. Cancer* **2007**, *43*, 1869. [Crossref]
48. Fu, C. K.; Chang, W. S.; Tsai, C. W.; Wang, Y. C.; Yang, M. D.; Hsu, H. S.; Chao, C. Y.; Yu, C. C.; Chen, J. C.; Pei, J. S.; Bau, D. T.; *Anticancer Res.* **2021**, *41*, 3309. [Crossref]
49. Dong, Z.; Guo, S.; Wang, Y.; Zhang, J.; Luo, H.; Zheng, G.; Yang, D.; Zhang, T.; Yan, L.; Song, L.; Liu, K.; Sun, Z.; Meng,

X.; Zheng, Z.; Zhang, J.; Zhao, Y.; *Onco Targets Ther.* **2020**, *13*, 8495. [Crossref]
50. Gold, J. M.; Raja, A.; *Cisplatin*; StatPearls Publishing: Treasure Island, USA, 2023. [Crossref] accessed in November 2023
51. Dasari, S.; Tchounwou, P. B.; *Eur. J. Pharmacol.* **2014**, *740*, 364. [Crossref]
52. Sun, W.; Xie, W.; Huang, D.; Cui, Y.; Yue, J.; He, Q.; Jiang, L.; Xiong, J.; Sun, W.; Yi, Q.; *Int. J. Mol. Med.* **2022**, *50*, 5. [Crossref]
53. Watabe, M.; Hishikawa, K.; Takayanagi, A.; Shimizu, N.; Nakaki, T.; *J. Biol. Chem.* **2004**, *279*, 6017. [Crossref]
54. Pagnan, A. L.; Pessoa, A. S.; Tokuhara, C. K.; Fakhoury, V. S.; Oliveira, G. S. N.; Sanches, M. L. R.; Inacio, K. K.; Ximenes, V. F.; Oliveira, R. C.; *Tissue Cell* **2022**, *74*, 101705. [Crossref]
55. Himelstein, B. P.; Canete-Soler, R.; Bernhard, E. J.; Dilks, D. W.; Muschel, R. J.; *Invasion Metastasis* **1995**, *14*, 246. [Link] accessed in November 2023
56. van Kempen, L. C. L.; Coussens, L. M.; *Cancer Cell* **2002**, *2*, 251. [Crossref]

Submitted: August 24, 2023
Published online: December 6, 2023